Journal of Photochemistry and Photobiology A: Chemistry 230 (2012) 47–54

Contents lists available at SciVerse ScienceDirect

Journal of Photochemistry and Photobiology A: Chemistry

journal homepage: www.elsevier.com/locate/jphotochem

Fluorine substituent effect on organic dyes for sensitized solar cells

Yan-Duo Lin, Tahsin J. Chow*

Institute of Chemistry, Academia Sinica, Taipei 115, Taiwan

ARTICLE INFO

Article history:
Received 31 August 2011
Received in revised form 1 December 2011
Accepted 25 December 2011
Available online 29 December 2011

Keywords:
Dye-sensitized solar cell
Stilbene
Fluorine substituted spacer
Charge transfer

ABSTRACT

Two sets of organic dyes containing a stilbene backbone with fluorine substituents were designed for a study on the quantum efficiency of dye-sensitized solar cells (DSSCs). The results revealed that adding a fluorine substituent on the phenyl group *ortho* to the cyanoacrylate can enhance the light-harvesting performance in comparison with the unsubstituted one. However, when the two *ortho*-positions were both substituted by fluorine atoms, the performance of DSSCs was substantially reduced. The reason was mainly ascribed to a distortion from a planar geometry caused by steric hindrance. The π-conjugation was therefore disturbed, and the result led to a substantial reduction of the short-circuit photocurrent density (J_{sc}). Another effect was found that the open-circuit photovoltage (V_{oc}) of the doubly substituted derivative was lower than that of the mono-substituted one. The more flexible conformation of the difluoro-substituted dyes induced an undesired nonradiative decay, therefore led to a reduction of open-circuit photovoltage. The phenomenon can be verified by electrochemical impendence spectrum. The non-planar geometry was realized by a computation using the density function theory (DFT) model. The slight blue shift of absorption band was also consistent with the calculated transition energy by a time dependent DFT model.

1. Introduction

Developing clean and renewable energy sources has become a global concern in recent years. Dye-sensitized solar cells (DSSCs) have attracted considerable attention due to their low manufacturing cost in comparison with traditional silicon-based solar cells [1,2]. Since the pioneering work by Grätzel and co-worker [3], many efficient transition–metal complexes [4–7] and metal-free organic dyes [8–18] have been reported. In general, the structure of organic dyes consists of a triphenylamine (TPA) moiety as an electron-donating group (D) and a cyanoacrylic acid as an electron acceptor (A). An intramolecular charge transfer can be induced across a π-conjugated spacer (S) upon photo-excitation. Among a variety of structural designs, the one using a stilbene as the S group, i.e., compound **H-P**, (Fig. 1) was reported to have achieved the highest quantum efficiency of $\eta = 9.1\%$ [19]. In order to further improve the efficiency of DSSCs, electron-withdrawing group such as fluorine has been incorporated onto S [20–22]. In a recent report it have been shown that adding a fluorine atom at the *ortho*-position to the cyanoacrylic acid can enhance the quantum efficiency, i.e., on the structures close resemblance to **F-P** and **H-P**. Encouraged by these results, we report herein the synthesis of two series of organic D–S–A dyads, in which one or two fluorine atoms are substituted on a phenyl group *ortho* to the cyanoacrylic acid acceptor. The effect of adding fluorine substituent is analyzed by comparing their DSSCs performances with the aid of theoretical computations.

2. Materials and methods

2.1. General information

The ^{1}H and ^{13}C NMR spectra were recorded on a Bruker 400 MHz spectrometer, and ^{19}F spectra were recorded on a Bruker 300 MHz spectrometer. Fast atom bombardment (FAB) mass spectra were recorded on a Jeol JMS 700 double-focusing spectrometer. UV spectra were measured on a Jasco V-530 double beam spectrophotometer. Fluorescence spectra were recorded on a Hitachi F-4500 fluorescence spectrophotometer. Compounds purchased from commercial sources were used as received. The syntheses of compounds **1N** [18], **1P** [19], **3PH** [19], and **H-P** [19] have been reported previously.

2.2. Synthesis

The synthetic pathways of the dyes are illustrated in Scheme 1. Compound **1** was coupled with commercially available 4-bromobenzaldehyde, 4-bromo-2-fluorobenzaldehyde, and 4-bromo-2,6-difluorobenzaldehyde (i.e., **2H**, **2F**, and **2FF**), respectively, by a Heck-type reaction to yield the corresponding

* Corresponding author at: 128 Academia Road Sec. 2, Nankang Taipei 115 Taiwan, ROC. Tel.: +886 2 2789 8637; fax: +886 2 2788 4179.
E-mail address: tjchow@chem.sinica.edu.tw (T.J. Chow).

1010-6030/$ – see front matter © 2011 Elsevier B.V. All rights reserved.
doi:10.1016/j.jphotochem.2011.12.013

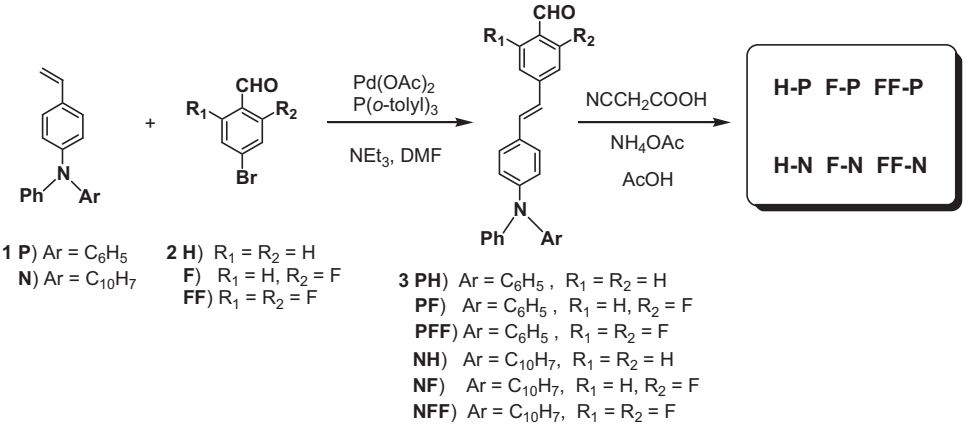

Scheme 1. Synthesis of the dyes.

compound of **3**. The aldehydes were condensed with cyanoacetic acid to afford the final products, i.e., the **P** and **N** series dyes, via Knöevenagel reaction in the presence of ammonium acetate.

2.3. General procedures for Heck reaction

A heterogeneous mixture of 0.28 ml of triethylamine, 1.00 ml of DMF, 1.05 mmol of styrene derivatives, 2 mol% of $Pd(OAc)_2/Pd_2(dba)_3$, 4 mol% of P(*o*-tolyl)$_3$, and 1.00 mmol of aryl bromide under argon were heated at 80 °C for 18 h. The solution was cooled and then 20 ml of CH_2Cl_2 was added. The insoluble residue was filtered off and the filtrate was concentrated in vacuo to afford a crude product. Further purification was performed by column chromatography.

2.4. General procedures for Knöevenagel condensation reaction

A mixture of aldehyde precursor (1.10 mmol), cyanoacetic acid (1.30 mmol), and ammonium acetate (0.28 mmol) in acetic acid (20 ml) was placed in a three-necked flask under nitrogen atmosphere and was stirred at 80 °C for 18 h. After cooling, the reaction was extracted with CH_2Cl_2. The organic layer was dried over anhydrous $MgSO_4$. The filtrate was concentrated under reduced pressure. Purification was performed by recrystallization in CH_2Cl_2/hexane.

2.5. (E)-4-(4-Diphenylaminostyryl)-2-fluorobenzaldehyde (*3PF*)

Compound **3PF** were synthesized via the typical Heck reaction procedure as described above. Purification was performed by silica gel column chromatograph eluted solvent CH_2Cl_2/hexane (1/5) to provide product **3PF** (1.07 g, 54% yield), mp: 88–89 °C. ^{1}H NMR (400 MHz, $CDCl_3$): δ 10.31 (s, 1H), 7.83 (d, 1H, J = 7.6 Hz), 7.41–7.34 (m, 3H), 7.31–7.26 (m, 5H), 7.22 (d, 1H, 7.0 Hz), 7.21–7.04 (m, 8H), 6.95 (d, 1H, J = 16.2 Hz). ^{13}C NMR (100 MHz, $CDCl_3$): δ 186.50, 166.41, 163.86, 148.63, 147.23, 146.49, 132.99, 129.66, 129.41, 128.98, 128.02, 124.99, 124.24, 123.60, 122.58, 113.12. ^{19}F NMR (282 MHz, $CDCl_3$): δ −123.16 (s, 1F). FAB-HRMS (*m*/*z*): 393.1529 (M^+) (calcd for $C_{27}H_{20}FNO$: 393.1526).

2.6. (E)-4-(4-Diphenylaminostyryl)-2,6-difluorobenzaldehyde (*3PFF*)

Compound **3PFF** were synthesized via the typical Heck reaction procedure as described above. Purification was performed by silica gel column chromatograph eluted solvent CH_2Cl_2/hexane (1/10) to provide product 3PFF (0.78 g, 42% yield), mp: 74–75 °C. ^{1}H NMR (400 MHz, $CDCl_3$): δ 10.29 (s, 1H), 7.38 (d, 2H, J = 8.7 Hz), 7.31–7.26 (m, 4H), 7.16–7.03 (m, 11H), 6.86 (d, 1H, J = 16.1 Hz). ^{13}C NMR (100 MHz, $CDCl_3$): δ 183.92, 164.82, 162.22, 149.01, 146.79, 134.18, 129.43, 128.92, 128.23, 125.13, 123.77, 123.14, 122.37, 112.25, 109.34. ^{19}F NMR (282 MHz, $CDCl_3$): δ −116.15 (s, 2F). FAB-HRMS (*m*/*z*): 412.1513 ($M+H^+$) (Calcd for $C_{27}H_{20}F_2NO$: 412.1523).

2.7. (E)-4-(4-(Naphthylphenylamino)styryl)benzaldehyde (3NH)

Compound **3NH** were synthesized via the typical Heck reaction procedure as described above. Column chromatography with ethyl acetate/hexane (1/10) as eluent afforded the yellow solid of **3NH** (0.79 g, 38% yield), mp: 162–163 °C. ^{1}H NMR (400 MHz, $CDCl_3$): δ 9.97 (s, 1H), 7.91 (d, 2H, J = 8.0 Hz), 7.85–7.79 (m, 3H), 7.60 (d, 2H, J = 8.2 Hz), 7.48 (d, 2H, J = 7.7 Hz), 7.39–7.35 (m, 4H), 7.35–7.21 (m, 3H), 7.16–7.00 (m, 2H), 7.00–6.95 (m, 4H). ^{13}C NMR (100 MHz, $CDCl_3$): δ 191.52, 148.88, 147.73, 143.97, 143.01, 135.32, 134.93, 131.87, 131.17, 130.22, 129.39, 129.25, 128.47, 127.84, 127.32,

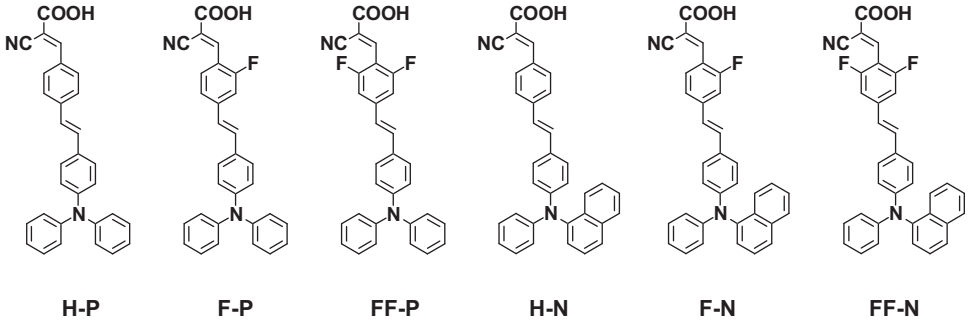

Fig. 1. The structures of organic dyes.

126.83, 126.54, 126.34, 126.24, 124.93, 124.08, 122.86, 122.64, 120.78. FAB-HRMS (m/z): 426.1867 ($M+H^+$) (calcd for $C_{31}H_{24}NO$: 426.1858).

*2.8. (E)-4-(4-(Naphthylphenylamino)styryl)-2-fluorobenzaldehyde (**3NF**)*

Compound **3NF** were synthesized via the typical Heck reaction procedure as described above. Purification was performed by silica gel column chromatograph eluted solvent CH_2Cl_2/hexane (1/25) to provide product **3NF** (0.53 g, 44% yield), mp: 90–91 °C. ^{1}H NMR (400 MHz, $CDCl_3$): δ 10.30 (s, 1H), 7.90 (d, 2H, J = 8.6 Hz), 7.83–7.80 (m, 2H), 7.48 (q, 2H, J = 7.6 Hz), 7.39–7.31 (m, 5H), 7.23–7.11 (m, 6H), 7.02–6.88 (m, 4H). ^{13}C NMR (100 MHz, $CDCl_3$): δ 186.49, 166.41, 163.85, 149.24, 147.58, 146.60, 142.89, 135.32, 133.11, 131.16, 129.29, 128.95, 128.75, 128.49, 128.06, 127.35, 126.93, 126.60, 126.35, 126.27, 124.03, 123.81, 123.07, 122.86, 122.39, 120.53, 113.03. ^{19}F NMR (282 MHz, $CDCl_3$): δ −123.24 (s, 1F). FAB-HRMS (m/z): 443.1676 (M^+) (calcd for $C_{31}H_{22}FNO$: 443.1685).

*2.9. (E)-4-(4-(Naphthylphenylamino)styryl)-2,6-difluorophenyl)benzaldehyde (**3NFF**)*

Compound **3NFF** were synthesized via the typical Heck reaction procedure as described above. Purification was performed by silica gel column chromatograph eluted solvent CH_2Cl_2/hexane (1/25) to provide product **3NFF** (0.66 g, 41% yield), mp: 97–98 °C. ^{1}H NMR (400 MHz, $CDCl_3$): δ 10.28 (s, 1H), 7.91–7.88 (m, 2H), 7.81 (d, 1H, J = 8.2 Hz), 7.51–7.46 (m, 2H), 7.39–7.32 (m, 4H), 7.27–7.23 (m, 2H), 7.17–7.13 (m, 3H), 7.04–7.02 (m, 3H), 6.94 (d, 2H, J = 8.6 Hz), 6.81 (d, 1H, J = 16.1 Hz). ^{13}C NMR (100 MHz, $CDCl_3$): δ 183.97, 164.86, 162.26, 149.61, 147.41, 146.77, 142.76, 135.32, 134.32, 131.13, 129.34, 128.52, 128.30, 128.05, 127.39, 127.04, 126.65, 126.36, 126.30, 123.97, 123.1862, 122.74, 120.28, 112.18, 109.27. ^{19}F NMR (282 MHz, $CDCl_3$): δ −116.24 (s, 2F). FAB-HRMS (m/z): 461.1584 (M^+) (calcd for $C_{31}H_{21}F_2NO$: 461.1584).

*2.10. (E)-3-(4-((E)-4-Diphenylaminostyryl)-2-florophenyl)-2-cyanoacrylic acid (**F-P**)*

Compound **F-P** was obtained according to the standard Knöevenagel condensation reaction as described above. Purification was performed by recrystallization in CH_2Cl_2/hexane to afford red solid (0.37 g, 79% yield), mp: 228–229 °C. ^{1}H NMR (400 MHz, $CDCl_3$): δ 8.59 (s, 1H), 8.48 (t, 1H, J = 7.9 Hz), 7.41–7.38 (m, 3H), .7.31–7.26 (m, 7H), 7.20–7.04 (m, 8H), 6.95 (d, 1H, J = 16.1 Hz). ^{13}C NMR (100 MHz, $CDCl_3$): δ 166.45, 163.95, 161.38, 148.84, 147.16, 146.99, 146.50, 146.40, 133.53, 129.43, 128.19, 125.09, 124.05, 123.71, 122.97, 122.52, 118.03, 115.25, 112.78, 112.55. ^{19}F NMR (282 MHz, $CDCl_3$): δ −112.79 (s, 1F). FAB-HRMS (m/z): 460.1587 (M^+) (Calcd for $C_{30}H_{21}FN_2O_2$: 460.1579).

*2.11. (E)-3-(4-((E)-4-Diphenylaminostyryl)-2,6-diflorophenyl)-2-cyanoacrylic acid (**FF-P**)*

Compound **FF-P** was obtained according to the standard Knöevenagel condensation reaction as described above. Purification was performed by recrystallization in CH_2Cl_2/hexane to afford red solid (0.58 g, 74% yield), mp: 226–227 °C. ^{1}H NMR (400 MHz, $CDCl_3$): δ 8.33 (s, 1H), 7.39 (d, 2H, J = 8.6 Hz), 7.31–7.26 (m, 5H), 7.15–7.03 (m, 10H), 6.88 (d, 2H, J = 16.1 Hz). ^{13}C NMR (100 MHz, $CDCl_3$): δ 165.30, 162.45, 159.89, 148.97, 14709, 145.46, 144.11, 133.89, 129.43, 129.01, 128.24, 125.12, 123.75, 123.17, 122.41, 113.73, 109.24, 108.49. ^{19}F NMR (282 MHz, $CDCl_3$): δ −104.87 (s, 2F). FAB-HRMS (m/z): 478.1585 ($M+H^+$) (Calcd for $C_{30}H_{21}F_2N_2O_2$: 479.1571).

*2.12. (E)-3-(4-((E)-4-(Naphthylphenylamino)styryl)phenyl)-2-cyanoacrylic acid (**H-N**)*

Compound **H-N** was obtained according to the standard Knöevenagel condensation reaction as described above. Purification was performed by recrystallization in CH_2Cl_2/hexane to afford red solid (1.00 g, 85% yield), mp: 201–202 °C. ^{1}H NMR (400 MHz, DMSO-d_6): δ 8.28 (s, 1H), 8.04–8.01 (m, 3H), 7.93 (d, 1H, J = 8.2 Hz), 7.84 (d, 1H, J = 8.4 Hz), 7.73 (d, 2H, J = 8.3 Hz), 7.61–7.37 (m, 7H), 7.30–7.26 (m, 2H), 7.13 (d, 1H, J = 16.3 Hz), 7.05–6.99 (m, 3H), 6.86 (d, 2H, J = 8.6 Hz) ppm. ^{13}C NMR (100 MHz, DMSO-d_6): δ 171.89, 163.44, 153.56, 148.14, 147.04, 142.42, 142.23, 134.90, 131.62, 131.28, 130.49, 129.89, 129.42, 128.57, 128.11, 127.30, 126.96, 126.66, 126.32, 124.86, 123.29, 122.67, 122.40, 120.04, 116.37, 101.93 ppm. FAB-HRMS (m/z): 493.1928 ($M+H^+$) (calcd for $C_{34}H_{25}N_2O_2$: 493.1916).

*2.13. (E)-3-(4-((E)-4-(Naphthylphenylamino)styryl)-2-fluorophenyl)-2-cyanoacrylic acid (**F-N**)*

Compound **F-N** was obtained according to the standard Knöevenagel condensation reaction as described above. Purification was performed by recrystallization in CH_2Cl_2/hexane to afford red solid (0.16 g, 76% yield), mp: 134–135 °C. ^{1}H NMR (400 MHz, DMSO-d_6): δ 8.29 (s, 1H), 8.21 (t, 1H, J = 7.8 Hz), 8.02 (d, 1H, J = 8.2 Hz), 7.93 (d, 1H, J = 8.2 Hz), 7.83 (d, 1H, J = 8.2 Hz), 7.63–7.38 (m, 9H), 7.30–7.26 (m, 2H), 7.14–7.00 (m, 4H), 6.85 (d, 2H, J = 7.8 Hz) ppm. ^{13}C NMR (100 MHz, DMSO-d_6): δ 171.92, 162.97, 162.68, 160.15, 148.45, 146.93, 145.32, 144.13, 142.15, 134.91, 133.01, 130.49, 129.47, 128.92, 128.79, 128.60, 128.34, 127.35, 127.04, 126.70, 126.35, 123.87, 123.27, 122.94 (d, J = 67.7 Hz), 122.61, 119.83, 117.65 (d, J = 45.0 Hz), 115.97, 112.61, 104.52 ppm. ^{19}F NMR (282 MHz, DMSO-d_6): δ −114.08 (s, 1F). FAB-HRMS (m/z): 510.1739 (M^+) (calcd for $C_{34}H_{23}FN_2O_2$: 510.1744).

*2.14. (E)-3-(4-((E)-4-(Naphthylphenylamino)styryl)-2,6-difluorophenyl)-2-cyanoacrylic acid (**FF-N**)*

Compound **FF-N** was obtained according to the standard Knöevenagel condensation reaction as described above. Purification was performed by recrystallization in CH_2Cl_2/hexane to afford red solid (0.39 g, 75% yield), mp: 133–134 °C. ^{1}H NMR (400 MHz, $CDCl_3$): δ 8.31 (s, 1H), 7.90 (d, 2H, J = 8.4 Hz), 7.81 (d, 1H, J = 8.2 Hz), 7.51–7.46 (m, 2H), 7.39–7.32 (m, 4H), 7.27–7.23 (m, 2H), 7.16–7.00 (m, 6H), 6.94 (d, 2H, J = 8.7 Hz), 6.83 (d, 1H, J = 16.1 Hz). ^{13}C NMR (100 MHz, $CDCl_3$): δ 176.92, 162.39, 159.83, 149.54, 147.42, 145.47, 143.92, 142.76, 135.30, 133.94, 131.11, 130.08, 129.31, 128.31, 127.87, 127.19, 126.64, 126.34, 126.29, 125.69, 123.97, 123.23, 123.04, 122.77, 120.31, 113.84, 105.15, 108.37. ^{19}F NMR (282 MHz, $CDCl_3$): δ −104.99 (s, 2F). FAB-HRMS (m/z): 528.1652(M^+) (calcd for $C_{34}H_{22}F_2N_2O_2$: 528.1649).

2.15. Device fabrication

A thin film of TiO_2 (16–18 μm thick) was coated on a 0.25 cm^2 FTO glass substrate. It was immersed in a THF solution containing 3×10^{-4} M dye sensitizers for 12 h, then rinsed with anhydrous acetonitrile and dried. Another piece of FTO with sputtering 100 nm

thick Pt was used as a counter electrode. The active area was controlled at a dimension of 0.25 cm^2 by adhering 60 μm thick polyester tape on the Pt electrode. The photocathode was placed on top of the counter electrode and was tightly clipped together to form a cell. Electrolyte was then injected into the seam between two electrodes. An acetonitrile solution containing LiI (0.5 M), I_2 (0.05 M), and 4-*tert*-butylpyridine (0.5 M) was used as the electrolyte. Devices made of a commercial dye N719 under the same condition was compared as a reference. The cell parameters were obtained under an incident light with intensity 100 mW cm^{-2}, which was generated by a 300 W Xe lamp passing through an AM 1.5 filter. The current–voltage parameters of DSSCs were recorded by a potentiostat/galvanostat model CHI650B (CH Instruments, USA).

2.16. Computation methods

The computations were performed with the Gaussian 03 program package [23]. The geometry was optimized by using B3LYP (Becke three parameters hybrid functional with Lee–Yang–Perdew correlation functionals) with the Pople 6-31G(d,p) atomic basis set [24,25]. The excitation transition of dyes were calculated using time-dependent density functional theory (TDDFT) calculations with B3LYP/6-31G(d,p).

3. Results and discussion

3.1. Absorption spectra

The absorption spectra of both the **P** and **N** series compounds in THF are shown in Fig. 2, the related photophysical and electrochemical data are summarized in Table 1. All dyes displayed two major absorption bands at 300–350 nm and 400–450 nm. The former is attributed to the π–π* transition, and the latter is assigned to the intramolecular charge transfer (ICT) transition from the triarylamine donors to the cyanoacrylic acid, as confirmed by the negative solvatochromic shifts in more polar solvents. This phenomenon may be ascribed to the deprotonation of the carboxylic group, which weakens the electron-withdrawing ability of the acceptor (see Figs. S1 and S2 in Supplementary data) [26,27]. The absorption maxima for monofluoro-substituted dyes, i.e., **F-N** and **F-P**, are not much different from those without the fluorine substituent. However, the absorption maxima for the difluoro-substituted dyes, i.e., **FF-N** and **FF-P**, exhibit a slight blue shift. It is likely caused by the steric hindrance between the two *ortho*-fluorine atoms and the cyanoacrylic acid, which twists the π-conjugation out of plane. The blue shift transition complies well with the result of computation according to the time-dependent density functional theory (TDDFT) (Table S1). The molar extinction coefficients of these dyes were in the range of 2.67–2.80 × 10^4 M^{-1} cm^{-1}, which is higher than that of N719

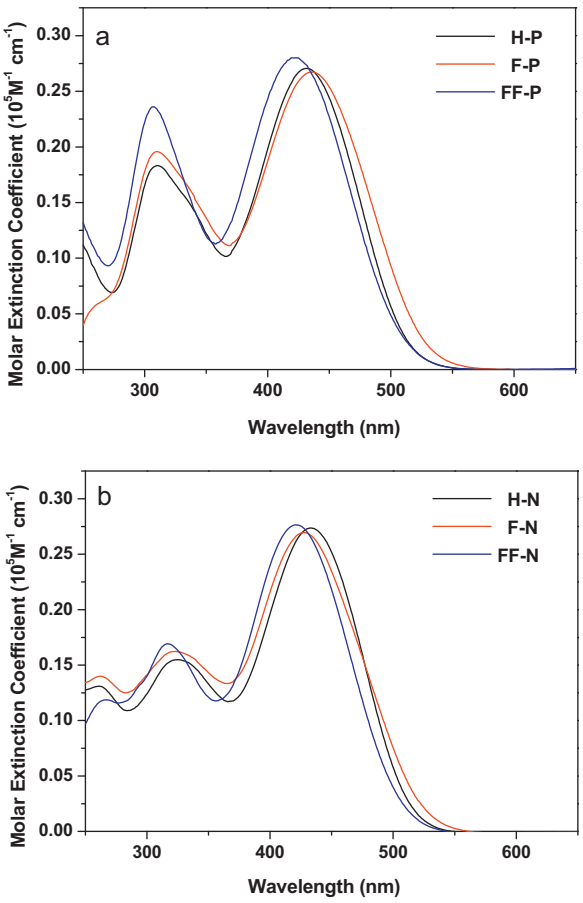

Fig. 2. Absorption spectra of (a) dye **P** (b) dye **N** in the THF solutions.

(1.41 × 10^4 M^{-1} cm^{-1}), revealing a good light harvesting nature. In Fig. 3 the spectra of dyes adsorbed on the TiO_2 surface are shown, and the corresponding data are collected in Table 1. The absorption maxima of these dyes display a blue-shift in comparison with those in solution. This blue shift is attributed to the deprotonation of carboxylic acid upon attaching to the TiO_2 surface, a similar effect to the negative solvatochromic shift in polar solvents [26,27].

3.2. Electrochemical properties

The redox potentials of all compounds were measured by cyclic voltammetry (CV) in THF solution containing 0.1 M tetrabutylammonium hexafluorophosphate ($TBAPF_6$) as the supporting electrolyte, $Ag/AgNO_3$ as the reference electrode, and a standard ferrocene/ferrocenium redox couple as an internal standard. The

Table 1
Photophysical and electrochemical data.

Compd	λ_{abs}[a] (nm)	λ_{max} ($\varepsilon \times 10^{-4}$, dm^3 mol^{-1} cm^{-1})[b]	λ_{fl}[c] (nm)	E_{0-0}[d] (nm)/(eV)	E_{ox}[e]/V	E_{LUMO}[f]/V
H-P	433 (400)	2.71	607	2.50	1.15	−1.35
F-P	436 (399)	2.67	615	2.51	1.19	−1.32
FF-P	422 (380)	2.80	620	2.55	1.20	−1.35
H-N	434 (406)	2.73	611	2.51	1.20	−1.31
F-N	427 (407)	2.69	600	2.52	1.21	−1.31
FF-N	421 (398)	2.76	611	2.55	1.19	−1.36

[a] Absorption maximum in THF, and that on TiO_2 in parentheses.
[b] Extinction coefficient in THF.
[c] Maximum of fluorescence in THF.
[d] Onset of the absorption spectra in THF.
[e] Oxidation potential measured vs Fc^+/Fc in THF were converted to normal hydrogen electrode (NHE) by addition of +0.63 V.
[f] Energy of LUMO estimated by $E_{ox} - E_{0-0}$.

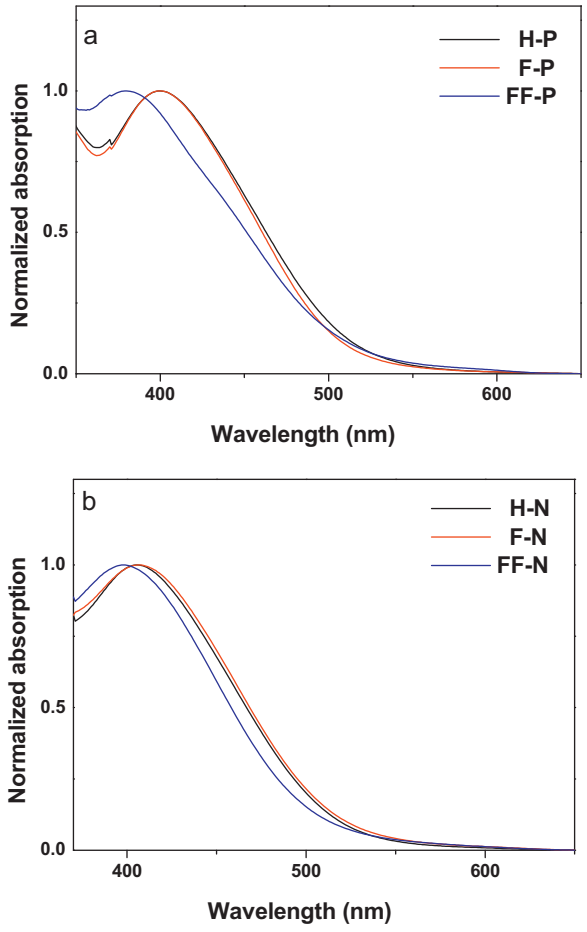

Fig. 3. Absorption spectra of (a) dye **P** (b) dye **N** adsorbed on the TiO_2 films.

potential level of highest occupied molecular orbital (HOMO) was estimated from the first oxidative wave (E_{ox}) as listed in Table 1. The results reveal that the HOMO levels of the dyes are all more positive than the I^-/I_3^- redox couple (~0.4 V versus NHE) and thus the regeneration of the oxidized dyes is thermodynamically feasible. The oxidation potentials of fluorine substituted dyes are found to be close to the corresponding unsubstituted ones (Table 1). The lowest unoccupied molecular orbital (LUMO) levels of the dyes were deduced from the first oxidation potential and the 0–0 transition energy (E_{0-0}) measured at the onset of the absorption spectrum. The LUMO levels of doubly substituted derivatives, i.e., **FF-P** and **FF-N**, are more negative than those of the mono-substituted ones, i.e., **F-P** and **F-N**. Nevertheless, their LUMO levels are more negative than the conduction band edge of the TiO_2 (−0.5 V versus NHE), which assure that the electron injection process is energetically favourable.

3.3. Fluorescence quantum yields and lifetime

The excited-state energy could be dissipated either through a radiative emission or through a nonradiative decay, i.e., torsional motion about a specific bond. In the present work the amount of non-radiative decay in the difluoro-substituted compounds was a crucial factor influencing the efficiency of DSSCs [18]. To verify the significance of non-radiative decay, kinetic parameters of the excited state are measured. From the fluorescence quantum yields and the lifetimes, the rate constant of nonradiative decay ($k_{nr} = (1 - \Phi_f)/\tau_f$) can be deduced.

Table 2
Fluorescence quantum yields (Φ_f), fluorescence decay times (τ_f), rate constants for fluorescence decay (k_f), and nonradiative decay (k_{nr}) for dyes **P** and **N** in THF.

Compd	Φ_f	τ_f (ns)	k_f (10^8 s^{-1})[a]	k_{nr} (10^8 s^{-1})[b]
H-P	0.22	2.29	0.96	3.41
F-P	0.19	2.42	0.79	3.35
FF-P	0.16	2.33	0.69	3.61
H-N	0.21	2.12	0.99	3.73
F-N	0.22	2.53	0.87	3.08
FF-N	0.17	2.15	0.79	3.86

[a] $k_f = \Phi_f/\tau_f$.
[b] $k_{nr} = (1 - \Phi_f)/\tau_f$.

The fluorescence quantum yields (Φ_f) and lifetimes (τ_f) of dyes **P** and **N** in THF are listed in Table 2, in which the τ_f values were determined at the emission maxima. All decay curves were fitted well into a single-exponential equation. The results showed that the values of k_{nr} for difluoro-substituted compounds, i.e., **FF-P** and **FF-N**, are greater than those of other dyes. It is also worthy of mentioning that the fluorescence lifetime of all dyes, i.e., around 2.12–2.53 ns, was significantly longer than the time needed for effective electron transfers from the dyes to the TiO_2 conductive band [28].

3.4. Photovoltaic performance of DSSCs

The optimized incident photo-to-current conversion efficiencies (IPCE) data of the dyes, obtained by using a sandwich cell comprising I_2 (0.05 M), LiI (0.5 M), and *tert*-butylpyridine (0.5 M) in acetonitrile as the redox electrolyte, are shown in Fig. 4. It is anticipated that the incorporation of *tert*-butylpyridine may

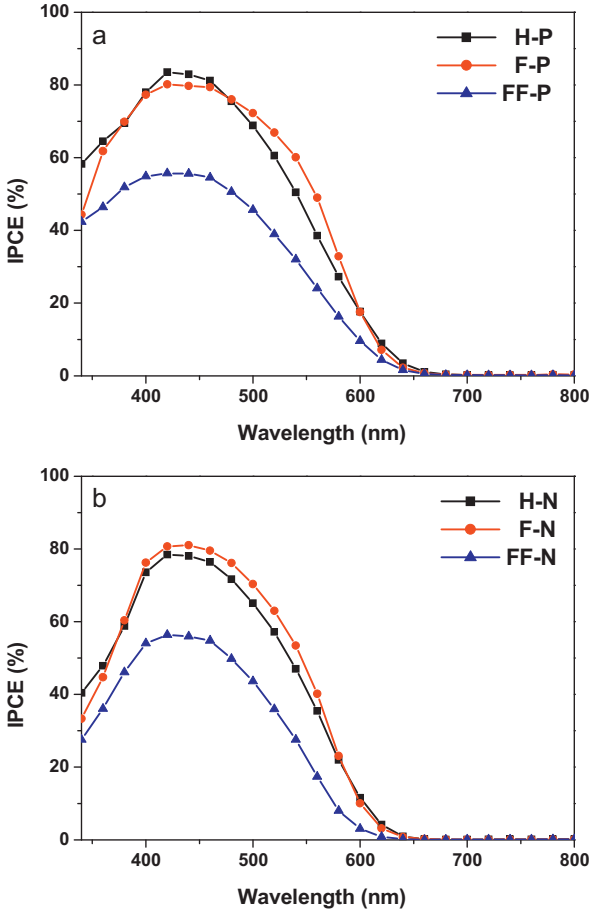

Fig. 4. The IPCE plots of DSSCs made with (a) dyes **P** and (b) dyes **N**.

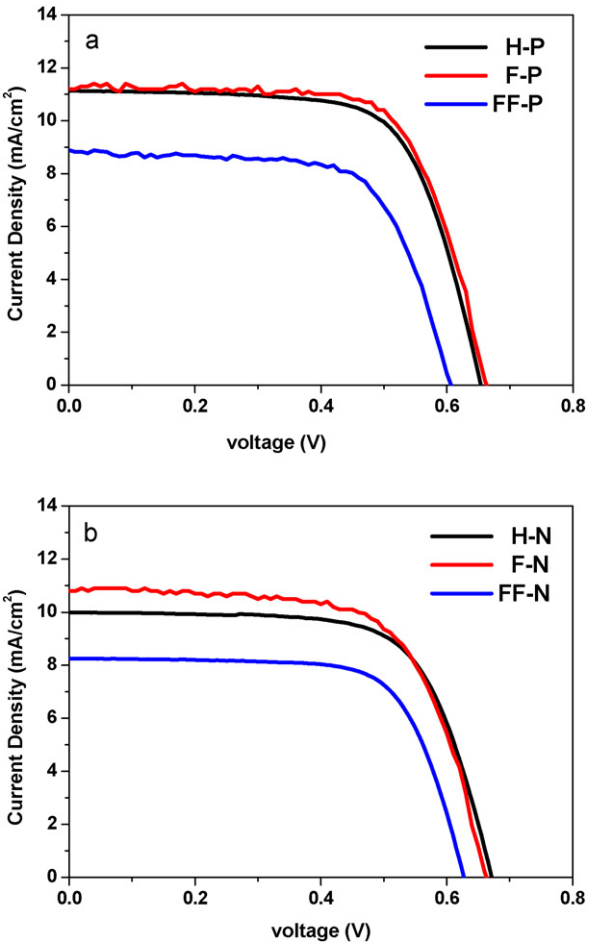

Fig. 5. Current–voltage plots for the DSSCs made with (a) dyes **P** and (b) dyes **N** under AM 1.5 G simulated solar light (100 mW cm^{-2}).

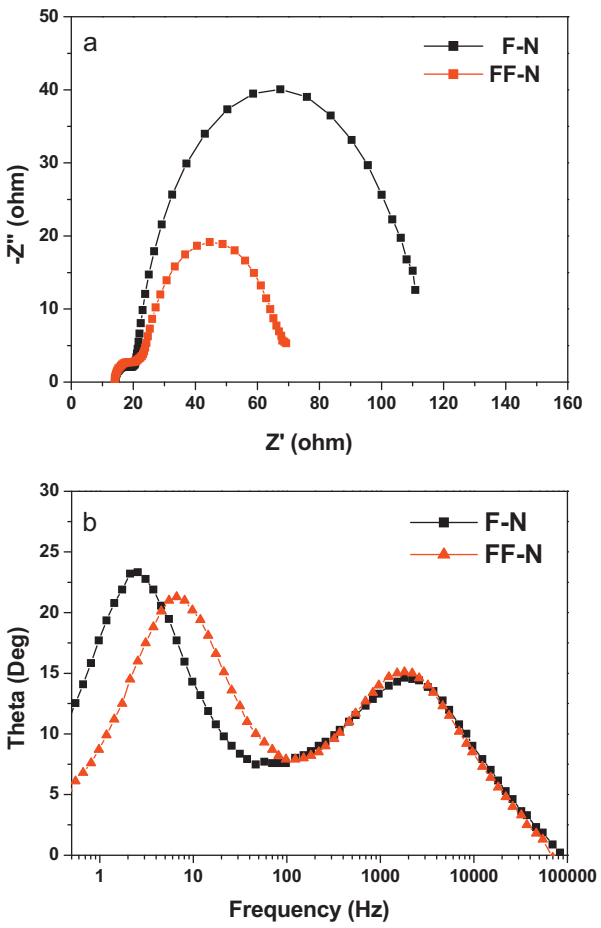

Fig. 6. The electrochemical impedance spectra of (a) Nyquist plots, and (b) Bode phase plots for the DSSCs made with **F-N** and **FF-N**.

have an effect of decreasing the dark current, thus enhancing the open-circuit photovoltage. The IPCE maxima of **H-P** and **F-P** were measured to be 83% and 80%, respectively, while those of **H-N** and **F-N** were 78% and 81%. The IPCE spectra of **FF** dyes were relatively low, e.g., 42–56% at 440 nm, compared with the unsubstituted ones.

The current–voltage (J–V) curves of the DSSCs under standard global AM 1.5 G irradiation is shown in Fig. 5. The open-circuit photovoltage (V_{oc}), short-circuit photocurrent density (J_{sc}), fill factor (ff), and solar-to-electrical energy conversion efficiencies (η) are summarized in Table 3, where N719 is included for a comparison. The overall performances of **F-P** and **F-N** were slightly better than those of the corresponding **H-P** and **H-N**. For FF dyes, the J_{sc} values are substantially lower than those of H and F dyes. It was ascribed to the twisted conformation between the difluorophenyl and cyanoacrylate moieties, which reduced the efficiency of π-conjugation.

Table 3
DSSCs performance parameters of dyes.[a]

Dye	Rel loading[b]	V_{oc} (mV)	J_{sc} (mA cm^{-2})	ff	η (%)
N719	0.89	0.76	14.59	0.63	7.00
H-P	1.00	0.66	11.12	0.68	4.98
F-P	1.02	0.67	11.20	0.69	5.19
FF-P	0.97	0.61	8.89	0.67	3.62
H-N	0.99	0.68	9.99	0.68	4.58
F-N	1.02	0.67	10.84	0.65	4.73
FF-N	0.96	0.64	9.21	0.68	4.01

[a] Experiments were conducted with TiO_2 photoelectrodes with approximately 16 μm thickness and 0.25 cm^2 working area on the FTO (8 Ω/sq.) substrates.
[b] The relative amount of dye absorption on TiO_2 relative to **H-P** (2.1×10^{-6} mol/cm^2).

The EIS of F and FF were performed in the dark under a forward bias to study the interfacial charge transfer processes. The small semicircle in the Nyquist plot (<20 Ω at the Z axis in Fig. 6a) corresponds to the electron transfer processes at the Pt/electrolyte interface, while the large semicircle (>20 Ω at the Z axis) corresponds to the electron transfer processes at the TiO_2/dye/electrolyte interface. The effectiveness of the dyes can be mainly reflected by the radius of the large semicircle. As indicated in Fig. 6 the radius for **FF-N** is significantly smaller than that of **F-N**, expressing its higher charge recombination rate in the dark. A larger dark current normally leads to a smaller value of V_{oc}, which is consistent with the observed performance of the device. A similar result can also be detected by the Bode plots. The higher-frequency peak (>100 Hz in Fig. 6b) represents the electron transfer processes at the Pt/electrolyte interface, while the lower frequency peak (<100 Hz) represents the electron transfer processes at the TiO_2/dye/electrolyte interface. From Fig. 6b it is clear that the position of high-frequency peaks for the two dyes did not change much. However, the lower frequency peak of **F-N** device shifted to a lower frequency than that of the **FF-N** device, an indication of a longer lifetime in the former [29,30].

3.5. Molecular orbital calculation

The electronic structures of the dyes were computed by DFT at B3LYP/6-31G(d,p) level with full geometry optimization. The optimized geometries of **H-P** and **F-P** adopt a nearly planar

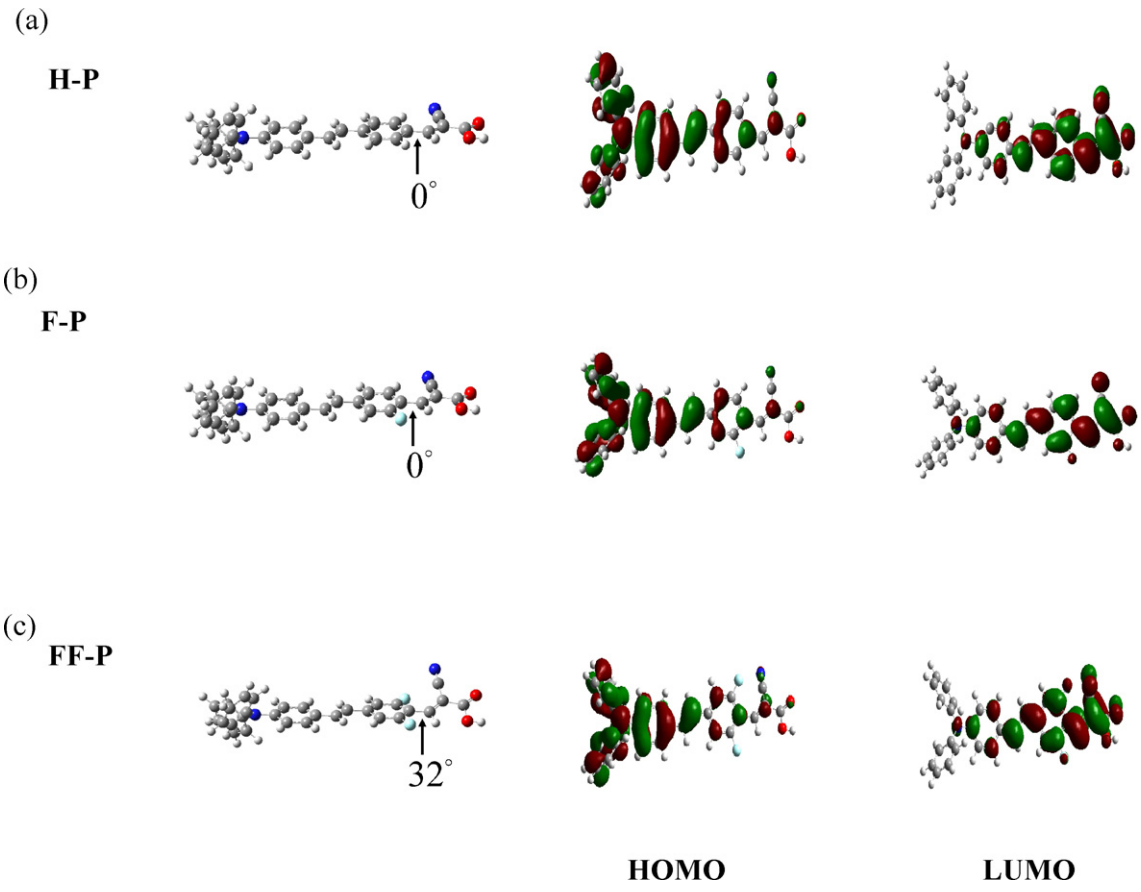

Fig. 7. Optimized geometry of **H-P** (top), **F-P** (middle) and **FF-P** (bottom), and the electronic maps of Frontier orbitals.

conformation, particularly between cyanoacrylic acid group and the adjacent phenyl ring (Fig. 7). The two fluorine substituents on the phenyl ring of **FF-P** induce a steric hindrance, thus a tortional angle of ca. 32° was twisted between the planes containing the cyanoacrylic acid group and the adjacent phenyl ring. The distorted nonplanar geometry of **FF-P** therefore reduces the degree of π-conjugation, and results to a blue-shift in the absorption spectra with respect to that of **H-P**. The calculated electron distributions of the frontier molecular orbitals for **H-P**, **F-P** and **FF-P** are shown in Fig. 7, and that for **H-N**, **F-N** and **FF-N** are shown in Fig. S3. In all the plots it shows that the HOMOs are mainly populated on the TPA moiety, while the LUMOs are on the cyanoacrylic acid group. The lowest energy transition from the TPA to the cyanoacrylic acid induces a charge separation along the long axis of the molecules. The electronic transitions were calculated by TDDFT for the lowest 10 singlet excitations on **H-P**, **F-P** and **FF-P**. The transitions with oscillator strength above 0.1 are summarized in Table S1. The lowest energy transitions, which correspond to charge transfers, exhibit high values of oscillator strength (0.93–0.97). The results correlated well with the large extinction coefficients in their absorption spectra.

4. Conclusions

A series of organic dyes containing fluoro-substituents on a phenyl group *ortho* to the cyanoacrylate acceptor were compared. The mono-fluorinated dyes showed similar V_{oc} and ff values to the non-substituted ones, yet showed larger J_{sc} values due to the extension of conjugation. As a result, the mono-fluorinated dyes exhibited better quantum efficiencies. In contrast, the difluorinated dyes showed a lower performance due to a twisted geometry between the difluorophenyl group and the cyanoacrylate moieties. The twisted geometry reduced the efficiency of π-conjugation, therefore reduced substantially the value of J_{sc}. The flexible conformation also resulted to a faster rate of charge recombination, which was evidenced by EIS and led to a lower value of V_{oc}. These results reveal that the advantage of adding electron-withdrawing substituents on the acceptor side may be voided by a slight distortion of molecular geometry. A delicate balance between the electronic and structure effect is necessary to achieve a high performance of DSSCs.

Acknowledgments

Financial supports were provided by the Institute of Chemistry, Academia Sinica, and the National Science Council of Taiwan.

Appendix A. Supplementary data

Supplementary data associated with this article can be found, in the online version, at doi:10.1016/j.jphotochem.2011.12.013.

References

[1] A. Hagfeldt, M. Grätzel, Light-induced redox reactions in nanocrystalline systems, Chem. Rev. 95 (1995) 49–68.
[2] A. Hagfeldt, G. Boschloo, L. Sun, L. Kloo, M. Grätzel, Dye-sensitized solar cells, Chem. Rev. 110 (2010) 6595–6663.
[3] B. O'Regan, M. Grätzel, A low-cost, high-efficiency solar cell based on dye-sensitized colloidal TiO_2 films, Nature 353 (1991) 737–740.
[4] M.K. Nazeeruddin, A. Kay, L. Rodicio, R. Humphry-Baker, E. Müller, P. Liska, N. Vlachopoulos, M. Grätzel, Conversion of light to electricity by cis-X_2Bis(2,2(-bipyridyl-4,4(-dicarboxylate)ruthenium(II) charge-transfer sensitizers (X = Cl^-, Br^-, I^-, CN^-, and SCN^-) on nanocrystalline TiO_2 electrodes, J. Am. Chem. Soc. 115 (1993) 6382–6390.

[5] M.K. Nazeeruddin, P. Péchy, T. Renouard, S.M. Zakeeruddin, R. Humphry-Baker, P. Comte, P. Liska, L. Cevey, E. Costa, V. Shklover, L. Spiccia, G.B. Deacon, C.A. Bignozzi, M. Grätzel, Engineering of efficient panchromatic sensitizers for nanocrystalline TiO_2-based solar cells, J. Am. Chem. Soc. 123 (2001) 1613–1624.
[6] C.-Y. Chen, J.-G. Chen, S.-J. Wu, J.-Y. Li, C.-G. Wu, K.-C. Ho, Multifunctionalized ruthenium-based supersensitizers for highly efficient dye-sensitized solar cells, Angew. Chem. Int. Ed. 47 (2008) 7342–7345.
[7] J.-F. Yin, J.-G. Chen, Z.-Z. Lu, K.-C. Ho, H.-C. Lin, K.-L. Lu, Toward Optimization of oligothiophene antennas: new ruthenium sensitizers with excellent performance for dye-sensitized solar cells, Chem. Mater. 22 (2010) 4392–4399.
[8] Y.J. Chang, T.J. Chow, Dye-sensitized solar cell utilizing organic dyads containing triarylene conjugates, Tetrahedron 65 (2009) 4726–4734.
[9] Y.J. Chang, T.J. Chow, Triaryl linked donor acceptor dyads for high-performance dye-sensitized solar cells, Tetrahedron 65 (2009) 9626–9632.
[10] D.-Y. Chen, K.-Y. Cheng, M.-L. Ho, I.-C. Wu, M.-W. Chung, H. Fu, P.-T. Chou, A new recognition concept using dye sensitized solar cell configuration, Chem. Commun. 47 (2011) 985–987.
[11] B.-S. Chen, Y.-J. Chen, P.-T. Chou, A new type of donor–acceptor dye bridged by the bidentate moiety; metal ion complexation enhancing DSSC performance, J. Mater. Chem. 21 (2011) 4090–4094.
[12] A. Mishra, M.K.R. Ficher, P. Bäuerle, Metal-free organic dyes for dye-sensitized solar cells: from structure: property relationships to design rules, Angew. Chem. Int. Ed. 48 (2009) 2474–2499.
[13] T.H. Kwon, V. Armel, A. Nattestad, D.R. MacFarlane, U. Bach, S.J. Lind, Dithienothiophene (DTT)-based dyes for dye-sensitized solar cells: synthesis of 2,6-dibromo-DTT, J. Org. Chem. 76 (2011) 4088–4093.
[14] Y. Numata, I. Ashraful, Y. Shirai, L. Han, Preparation of donor–acceptor type organic dyes bearing various electron-withdrawing groups for dye-sensitized solar cell application, Chem. Commun. 47 (2011) 6159–6161.
[15] H. Im, S., Kim, C, Park S.-H. Jang, C.-J. Kim, K., Kim, N.-G. Park, C. Kim, High performance organic photosensitizers for dye-sensitized solar cells, Chem. Commun. 46 (2010) 1335-1337.
[16] S.-H. Lin, Y.-C. Hsu, J.T. Lin, C.-K. Lin, J.-S. Yang, Isotruxene-derived cone-shaped organic dyes for dye-sensitized solar cells, J. Org. Chem. 75 (2010) 7877–7886.
[17] Y.-D. Lin, C.-T. Chien, S.-Y. Lin, H.-H. Chang, C.-Y. Liu, T.J. Chow, Meta versus para substituent effect of organic dyes for sensitized solar cells, J. Photochem. Photobiol. A 222 (2011) 192–202.
[18] Y.-D. Lin, T.J. Chow, Geometrical effect of stilbene on the performance of organic dye-sensitized solar cells, J. Mater. Chem. 21 (2011) 14907–14916.
[19] S. Hwang, J.H. Lee, C. Park, H. Lee, C. Kim, C. Park, M.-H. Lee, W. Lee, J. Park, K. Kim, N.-G. Park, C. Kim, A highly efficient organic sensitizer for dye-sensitized solar cells, Chem. Commun. (2007) 4887–4889.
[20] B.-S. Chen, D.-Y. Chen, C.-L. Chen, C.-W. Hsu, H.-C. Hsu, K.-L. Wu, S.-H. Liu, P.-T. Chow, Donor–acceptor dyes with fluorine substituted phenylene spacer for dye-sensitized solar cells, J. Mater. Chem. 21 (2011) 1937–1945.
[21] D.-Y. Chen, Y.-Y. Hsu, H.-C. Hsu, B.-S. Chen, Y.-T. Lee, H. Fu, Organic dyes with remarkably high absorptivity; all solid-state dye sensitized solar cell and role of fluorine substitution, Chem. Commun. 46 (2010) 5256–5258.
[22] Y.J. Chang, T.J. Chow, Highly efficient triarylene conjugated dyes for sensitized solar cells, J. Mater. Chem. 21 (2011) 9523–9531.
[23] M.J. Frisch, G.W. Trucks, H.B. Schlegel, G.E. Scuseria, M.A. Robb, J.R. Cheeseman, J.A. Montgomery Jr., T. Vreven, K.N. Kudin, J.C. Burant, J.M. Millam, S.S. Iyengar, J. Tomasi, V. Barone, B. Mennucci, M. Cossi, G. Scalmani, N. Rega, G.A. Petersson, H. Nakatsuji, M. Hada, M. Ehara, K. Toyota, R. Fukuda, J. Hasegawa, M. Ishida, T. Nakajima, Y. Honda, O. Kitao, H. Nakai, M. Klene, X. Li, J.E. Knox, H.P. Hratchian, J.B. Cross, V. Bakken, C. Adamo, J. Jaramillo, R. Gomperts, R.E. Stratmann, O. Yazyev, A.J. Austin, R. Cammi, C. Pomelli, J.W. Ochterski, P.Y. Ayala, K. Morokuma, G.A. Voth, P. Salvador, J.J. Dannenberg, V.G. Zakrzewski, S. Dapprich, A.D. Daniels, M.C. Strain, O. Farkas, D.K. Malick, A.D. Rabuck, K. Raghavachari, J.B. Foresman, J.V. Ortiz, Q. Cui, A.G. Baboul, S. Clifford, J. Cioslowski, B.B. Stefanov, G. Liu, A. Liashenko, P. Piskorz, I. Komaromi, R.L. Martin, D.J. Fox, T. Keith, M.A. Al-Laham, C.Y. Peng, A. Nanayakkara, M. Challacombe, P.M.W. Gill, B. Johnson, W. Chen, M.W. Wong, C. Gonzalez, J.A. Pople, Gaussian 03, Gaussian Inc., Pittsburgh, PA, 2003.
[24] A.D. Becke, Density-functional thermochemistry. III. The role of exact exchange, J. Chem. Phys. 98 (1993) 5648–5652.
[25] R. Ditchfield, W.J. Hehre, J.A. Pople, Self-consistent molecular-orbital methods. IX. An extended gaussian-type basis for molecular-orbital studies of organic molecules, J. Chem. Phys. 54 (1971) 724–728.
[26] Z. Wang, Y. Cui, Y. Dan-oh, C. Kasada, A. Shinpo, K. Hara, Thiophene-functionalized coumarin dye for efficient dye-sensitized solar cells: electron lifetime improved by coadsorption of deoxycholic acid, J. Phys. Chem. C 111 (2007) 7224–7230.
[27] H.-Y. Yang, Y.-S. Yen, Y.-C. Hsu, H.-H. Chou, J.T. Lin, Organic dyes incorporating dithieno[3,2-b:2(,3(-d]thiophene moiety for efficient dye-sensitized solar cells, Org. Lett. 12 (2010) 16–19.
[28] S.E. Koops, B.C. O'Regan, P.R.F. Barnes, J.R. Durrant, Parameters influencing the efficiency of electron injection in dye-sensitized solar cells, J. Am. Chem. Soc. 131 (2009) 4808–4818.
[29] M. Adachi, M. Sakamoto, J. Jiu, Y. Ogata, S. Isoda, Determination of parameters of electron transport in dye-sensitized solar cells using electrochemical impedance spectroscopy, J. Phys. Chem. B 110 (2006) 13872–13880.
[30] Q. Wang, J. Moser, M. Grätzel, Electrochemical impedance spectroscopic analysis of dye-sensitized solar cells, J. Phys. Chem. B 109 (2005) 14945–14953.